Published for SISSA by Springer

Received: *May 11, 2017*
Revised: *July 6, 2017*
Accepted: *July 12, 2017*
Published: *August 21, 2017*

NLO predictions for Higgs boson pair production with full top quark mass dependence matched to parton showers

G. Heinrich,[a] **S.P. Jones,**[a] **M. Kerner,**[a] **G. Luisoni**[b] **and E. Vryonidou**[c]

[a] *Max Planck Institute for Physics, Föhringer Ring 6, 80805 München, Germany*
[b] *Theoretical Physics Department, CERN, Geneva, Switzerland*
[c] *Nikhef, Science Park 105, 1098 XG, Amsterdam, The Netherlands*

E-mail: gudrun@mpp.mpg.de, sjones@mpp.mpg.de, kerner@mpp.mpg.de, gionata.luisoni@cern.ch, eleniv@nikhef.nl

Abstract: We present the first combination of NLO QCD matrix elements for di-Higgs production, retaining the full top quark mass dependence, with a parton shower. Results are provided within both the POWHEG-BOX and MadGraph5_aMC@NLO Monte Carlo frameworks. We assess in detail the theoretical uncertainties and provide differential results. We find that, as expected, the shower effects are relatively large for observables like the transverse momentum of the Higgs boson pair, which are sensitive to extra radiation. However, these shower effects are still much smaller than the differences between the Born-improved HEFT approximation and the full NLO calculation in the tails of the distributions.

Keywords: NLO Computations, QCD Phenomenology

ArXiv ePrint: 1703.09252

https://doi.org/10.1007/JHEP08(2017)088

JHEP08(2017)088

Contents

JHEP08(2017)088

1 Introduction

Exploring the Higgs sector is one of the major goals for the next phases of LHC experiments. In particular, the form of the Higgs potential as predicted by the Standard Model (SM) needs to be confirmed. While one important parameter of the potential, the Higgs boson mass, has been measured already to an impressive accuracy, the Higgs boson self-coupling is still only very weakly constrained. The latter can be measured for example via Higgs boson pair production in gluon fusion, which is the dominant production mechanism of Higgs boson pairs. However, the cross section is about 1000 times smaller than that for single Higgs production, which makes the measurement very challenging even with the high luminosity upgrade of the LHC. This fact on the other hand makes this channel very interesting for New Physics searches, as the delicate cancellations between different contributions which happen in the SM are altered in most New Physics models, leading to potentially large effects.

At the LHC, the decay channel $HH \to b\bar{b}\gamma\gamma$ has so far led to the most stringent limit on the di-Higgs production cross section of $\sigma/\sigma_{\rm SM} \leq 19$ in CMS [1], while the ATLAS collaboration achieved the most restrictive upper bound of $\sigma/\sigma_{\rm SM} \leq 29$ in the $b\bar{b}b\bar{b}$ decay channel [2]. A previous combination of various decay channels measured in the ATLAS detector led to $\sigma/\sigma_{\rm SM} \leq 70$ [4]. The CMS collaboration also produced new limits for resonant and non-resonant Higgs boson pair production in the $bbWW$ and $bb\tau\tau$ channels [3, 5].

On the theory side, the leading order calculation of Higgs boson pair production in gluon fusion, which proceeds via heavy quark loops, has been performed in refs. [6–8]. Higher order corrections were for a long time available only within the Higgs Effective Field Theory

(HEFT) approximation, where the NLO corrections are calculated in the $m_t \to \infty$ limit, leading to point-like effective couplings of gluons to Higgs bosons. In ref. [9] NLO corrections were calculated in the so-called "Born-improved HEFT" approximation, where the basic HEFT result is rescaled by a factor $B_{\mathrm{FT}}/B_{\mathrm{HEFT}}$, B_{FT} denoting the leading order matrix element squared in the full theory.

In refs. [10, 11], an approximation called "$\mathrm{FT}_{\mathrm{approx}}$" was introduced, which contains the full top quark mass dependence in the real radiation, while the virtual part is calculated in the HEFT approximation and rescaled at the event level by the re-weighting factor $B_{\mathrm{FT}}/B_{\mathrm{HEFT}}$.

In addition, the HEFT results at NLO and NNLO have been improved by an expansion in $1/m_t^{2\rho}$ in refs. [12–15], with $\rho^{\max} = 6$ at NLO, and $\rho^{\max} = 2$ for the soft-virtual part at NNLO [14].

The NNLO QCD corrections in the heavy top limit have been computed in refs. [13, 16–18], and they have been supplemented by an expansion in $1/m_t^2$ in ref. [14] and by resummation, at NLO+NNLL in ref. [19] and at NNLO+NNLL in ref. [20], leading to K-factors of about 1.2 relative to the Born-improved HEFT result.

Very recently, the full NLO corrections, including the top quark mass dependence also in the virtual two-loop amplitudes, have been calculated [21, 22] and compared to previous approximations for various observables [23]. The full NLO calculation was supplemented by NLL resummation in ref. [24].

Numerous phenomenological studies of Higgs boson pair production have been performed both within and beyond the SM [25–54]. Further, it also has been suggested recently to obtain constraints on the Higgs boson self-coupling from electroweak corrections to single Higgs boson production [55–57].

The studies of Higgs boson pair production mentioned above usually had at least one of the following drawbacks: either they are based on leading order matrix elements, while including the full top quark mass dependence, or the matrix elements include higher orders in QCD but have been performed within the infinite-top-mass approximation, which is known to fail at scales where the top quark loops are resolved [21, 23, 58].

Results for Higgs boson pair production merged to $HH + 1$ jet matrix elements at leading order, with full top and bottom quark mass dependence, matched to a parton shower within `HERWIG++`, have been presented in ref. [59]. The "$\mathrm{FT}_{\mathrm{approx}}$" [11] calculation includes the matching of di-Higgs production to a parton shower [10] keeping the full top quark mass dependence in the real radiation, while the virtual part is calculated in the Born-improved HEFT approximation.

In this paper, we present the first combination of the full NLO calculation, including the full top quark mass dependence at two loops, with a parton shower, within both the `POWHEG-BOX` [60, 61] and the `MadGraph5_aMC@NLO` framework [62, 63]. This allows us to compare the `POWHEG` [60] and `MC@NLO` [64] matching schemes while using the same `Pythia 8` [65, 66] shower in both cases. We also investigate the PDF and scale uncertainties and calculate observables like the di-Higgs p_T spectrum, p_T^{hh}, where fixed order NLO calculations cannot give a satisfactory description at low p_T^{hh}. Further, we discuss the possibility to infer the leading contribution of a full NNLO calculation from the showered

JHEP08(2017)088

results, based on a comparison of the NNLO calculation in the HEFT approximation [18] with the showered results.

2 Details of the calculation

In this section we present the details of the implementation of the calculation within the POWHEG-BOX Monte Carlo program. The results from MG5_aMC@NLO presented in the next sections are based on a similar implementation. Both codes use the same grid for the virtual two-loop amplitude discussed in section 2.1. Further details about the calculation based on Born-improved HEFT and $\mathrm{FT}_{\mathrm{approx}}$ within MG5_aMC@NLO already have been published elsewhere [10, 11].

In order to allow for comparisons and cross checks, we implemented both the effective theory as well as the full SM amplitudes at NLO. This allows to run the code in four different modes by changing the flag mtdep in the POWHEG-BOX run card. The possible choices and the corresponding calculation, as presented in the previous section, are the following:

mtdep=0: computation using basic HEFT,

mtdep=1: computation using Born-improved HEFT,

mtdep=2: computation in the approximation $\mathrm{FT}_{\mathrm{approx}}$ (full mass dependence in the Born and in the real radiation, Born-improved HEFT for the virtual part),

mtdep=3: computation in the full SM.

The corresponding modes are also available in MG5_aMC@NLO.

The leading order amplitude in the full theory and all the amplitudes in the HEFT were implemented analytically, whereas the one-loop real radiation contribution and the two-loop virtual amplitudes in the full SM rely on numerical or semi-numerical codes. Since the virtual two-loop amplitudes in the full theory are computed keeping the Higgs bosons on-shell, we assume a vanishing Higgs boson width in all the modes listed above. Higgs boson decays can be computed in the narrow width approximation by the parton shower. In the next sections we give some more details about our implementation. We will use the term "HEFT approximation", or simply "HEFT", for basic HEFT, while results in the Born-improved HEFT will be denoted by "B-i. HEFT".

2.1 Virtual two-loop amplitudes

For the virtual two-loop amplitudes, we have used the results of the calculation presented in refs. [21, 23], which is based on an extension of the program GoSam [67] to two loops [68], using also Reduze 2 [69] and SecDec 3 [70].

The values for the Higgs boson and top quark masses have been set to $m_h = 125\,\mathrm{GeV}$ and $m_t = 173\,\mathrm{GeV}$, such that the two-loop amplitudes only depend on two independent variables, the Mandelstam invariants $\hat{s}$ and $\hat{t}$. We have constructed a grid in these variables together with an interpolation framework, such that an external program can call the

JHEP08(2017)088

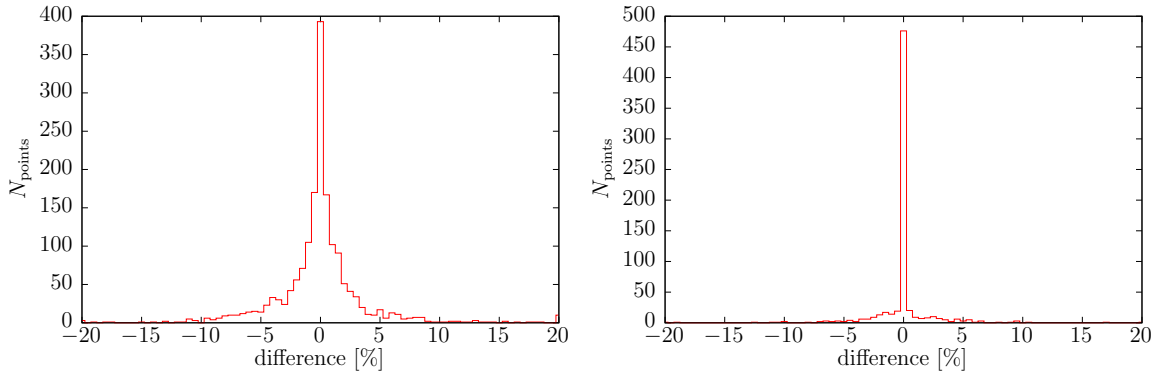

Figure 1. Closure test of the grid interpolation. The left (right) plot shows the relative difference of the grid results compared to a grid obtained from 50% (80%) of the input data points, evaluated at the remaining data points. Differences are defined as positive (negative) if the full grid yields larger (smaller) results. The outermost bins contain all results with differences larger than 20%.

virtual two-loop amplitude at any phase space point without having to do costly two-loop integrations.

In more detail, we first transform the Mandelstam invariants $\hat{s}$ and $\hat{t}$ to new variables

$$x = f\big(\beta(\hat{s})\big)\,, \quad \text{with} \quad \beta = \left(1 - \frac{4m_h^2}{\hat{s}}\right)^{\frac{1}{2}} \tag{2.1}$$

$$c_\theta = |\cos\theta| = \left|\frac{\hat{s} + 2\hat{t} - 2m_h^2}{\hat{s}\beta(\hat{s})}\right|, \tag{2.2}$$

where f can, in principle, be any strictly increasing function. Setting $f(\beta)$ according to the cumulative distribution function of the phase space points used in our original calculation, we obtain a nearly uniform distribution of these points in the (x, c_θ) unit square. Instead of a direct interpolation of the phase space points, we chose to apply a two-step procedure: first, we generate a regular grid with a fixed grid spacing in the variables x and c_θ, where we estimate the result at each grid point applying a linear interpolation of our original results in the vicinity of the specific grid point. In a second step, we apply Clough-Tocher interpolation [71] as implemented in the python *SciPy* package [72]. Applying this procedure reduces the size of interpolation artefacts, which we obtain due to the numerical uncertainty of our two-loop results. In figure 1 we test how omitting input data points influences the results of the grid interpolation. Removing 20% of the input data points changes the interpolation results by less than 0.25% for 70% of the tested points. Differences larger than 5% are obtained for 6% of the results.

We should point out that the grid is constructed from a sample of phase space points which is based on runs at $\sqrt{s} = 14\,\text{TeV}$. Therefore, even though the grid is not explicitly dependent on the centre-of-mass energy, one should be aware of the fact that for runs at e.g. 100 TeV, the grid may not be reliable for points with large $\hat{s}$ due to a lack of statistics in this region upon construction.

In our original calculation [21, 23], we used Catani-Seymour dipole subtraction [73] for the real radiation. The finite combination of the renormalized virtual amplitude $\mathcal{V}_b$ with

JHEP08(2017)088

the Catani-Seymour **I**-operator can be straightforwardly converted into the quantity $\mathcal{V}_{\rm fin}$ of refs. [61, 74], defined by

$$\mathcal{V}_b = \mathcal{N}\,\frac{\alpha_s}{2\pi}\left[\frac{1}{\epsilon^2}\,a\,\mathcal{B} + \frac{1}{\epsilon}\sum_{i,j} c_{ij}\,\mathcal{B}_{ij} + \mathcal{V}_{\rm fin}\right], \tag{2.3}$$

$$\mathcal{N} = \frac{(4\pi)^\epsilon}{\Gamma(1-\epsilon)}\left(\frac{\mu_r^2}{Q^2}\right)^\epsilon. \tag{2.4}$$

For this process the colour-correlated Born squared amplitudes $\mathcal{B}_{12}$ and $\mathcal{B}_{21}$ are equal and we have $a = 2C_A$ and $c_{12} = c_{21} = \beta_0/2$. In the `POWHEG-BOX` and `MG5_aMC@NLO` frameworks the arbitrary scale Q is chosen as μ_r. Specifically, we obtain

$$\begin{aligned}\mathcal{V}_{\rm fin}(\mu_r) = {}& \frac{2\pi}{\alpha_s(\mu_r)}(\mathcal{V}_b + \mathbf{I}\otimes\mathcal{B})(\mu_r) \\ & - \mathcal{B}(\mu_r)\left(C_A \ln^2\left(\frac{\mu_r^2}{\hat{s}}\right) + \beta_0 \ln\left(\frac{\mu_r^2}{\hat{s}}\right) + \beta_0 + 2K_g - \frac{2\pi^2}{3}C_A\right).\end{aligned} \tag{2.5}$$

The grid evaluates $\mathcal{V}_{\rm fin}$ at the scale $\mu_0 = \sqrt{\hat{s}}/2$ and the results for an arbitrary scale can be obtained from the relation

$$\mathcal{V}_{\rm fin}(\mu_r) = \mathcal{V}_{\rm fin}(\mu_0)\cdot\frac{\mathcal{B}(\mu_r)}{\mathcal{B}(\mu_0)} + C_A\mathcal{B}(\mu_r)\left(\ln^2\left(\frac{\mu_0^2}{\hat{s}}\right) - \ln^2\left(\frac{\mu_r^2}{\hat{s}}\right)\right). \tag{2.6}$$

The Born amplitude $\mathcal{B}$ and the colour-correlated Born amplitudes $\mathcal{B}_{ij}$ in (2.3) are evaluated in $D = (4-2\epsilon)$ dimensions using conventional dimensional regularization (CDR). As all formulas for the soft contributions and the collinear remnants used in the `POWHEG-BOX` and `MG5_aMC@NLO` are computed in the $\overline{\rm MS}$ scheme, using CDR, constructing $\mathcal{V}_{\rm fin}$ according to (2.5) ensures the treatment is consistent with that implemented in the Monte Carlo programs.

2.2 Real radiation and parton shower matching

The real radiation matrix elements in the full SM were implemented using the interface [75] between `GoSam` [67, 76] and the `POWHEG-BOX` [60, 61], modified accordingly to compute the real corrections instead of the virtual ones. The one-loop real amplitudes we generated with the new version 2.0 of `GoSam` [67], that uses `QGRAF` [77], `FORM` [78] and `Spinney` [79] for the generation of the Feynman diagrams, and offers a choice from `Samurai` [80, 81], `golem95C` [82–84] and `Ninja` [85, 86] for the reduction. At run time the amplitudes were computed using `Ninja` [85, 86] and `OneLOop` [87] for the evaluation of the scalar one-loop integrals.

In order to avoid numerical instabilities in the one-loop real matrix elements in the limit where the additional parton becomes soft and/or collinear, a technical cut $p_T^{\rm hh} > 10^{-3}$ GeV has been introduced. We carefully checked that the total cross section does not change significantly when varying the cut value.

Within `MG5_aMC@NLO`, the one-loop born and real amplitudes are computed using `MadLoop` [88], which in turn exploits `CutTools` [89], `Ninja` [86, 90] or `Collier` [91], together

JHEP08(2017)088

with an in-house implementation of the OpenLoops optimisation [92]. In MG5_aMC@NLO, the computation is based on event reweighting, as described in [10, 11]. This functionality in MG5_aMC@NLO has since been automated as documented in [93]. In practice, the HEFT is used to generate the events at NLO which are then reweighted to introduce the full top quark mass dependence of the one- and two-loop amplitudes.

In order to study the phenomenological impact of the two different matching schemes implemented in the POWHEG-BOX and in MG5_aMC@NLO, we compare the two results using the same parton shower. In both cases we use Pythia 8.2 with the same settings to produce showered events from both the POWHEG-BOX and the MG5_aMC@NLO results at LHE level. This means that the differences in the distributions produced by POWHEG and MG5_aMC@NLO respectively, will only be due to the corresponding matching schemes.

3 Results

In this section we present phenomenological results and compare predictions at different levels. We start presenting some consistency checks at the fixed order level and at the Les Houches event level (LHE), i.e. after the first hard emission is generated according to the POWHEG method. To assess the impact of the parton shower and estimate its capacity to include approximate higher order effects, in section 3.3 we compare results in the basic HEFT approximation at NLO+PS with the NNLO predictions from reference [94]. Finally, in section 3.4 NLO and NLO+PS results in the full SM are presented.

All the results we computed using the PDF4LHC15_nlo_30_pdfas [95–98] parton distribution functions interfaced to our codes via LHAPDF [99], along with the corresponding value for α_s. The masses of the Higgs boson and the top quark have been set, as in the virtual amplitude, to $m_h = 125\,\text{GeV}$, $m_t = 173\,\text{GeV}$, respectively, whereas their widths have been set to zero. As already mentioned in the previous section, we consider on-shell Higgs bosons and leave the analysis of more exclusive final states, stemming from Higgs boson decays, to future studies. Jets are clustered with the anti-k_T algorithm [100] as implemented in the Fastjet package [101, 102], with jet radius $R = 0.4$ and a transverse momentum greater than $p_{T,\text{min}}^{\text{jet}} = 20\,\text{GeV}$. The theoretical scale uncertainty is estimated by varying the factorization scale μ_F and the renormalization scale μ_R. The scale variation bands are obtained by computing the envelopes of a 7-point scale variation around the central scale $\mu_0 = m_{\text{hh}}/2$, with $\mu_{R,F} = c_{R,F}\,\mu_0$, where $c_R, c_F \in \{2, 1, 0.5\}$. The extreme variations $(c_R, c_F) = (2, 0.5)$ and $(c_R, c_F) = (0.5, 2)$ have been omitted.

We also have varied the PDFs using the 30 error PDFs contained in the PDF4LHC15_nlo_30_pdfas set and found that the uncertainty due to PDF variations never exceeds 6% and therefore is well below the scale variation uncertainty. The uncertainty bands shown on our results originate from scale variations only.

We should point out that we switched off the hadronisation and the multiple interactions in the parton shower. A detailed phenomenological study including various Higgs boson decay channels as well as hadronisation effects will be left to a subsequent publication.

JHEP08(2017)088

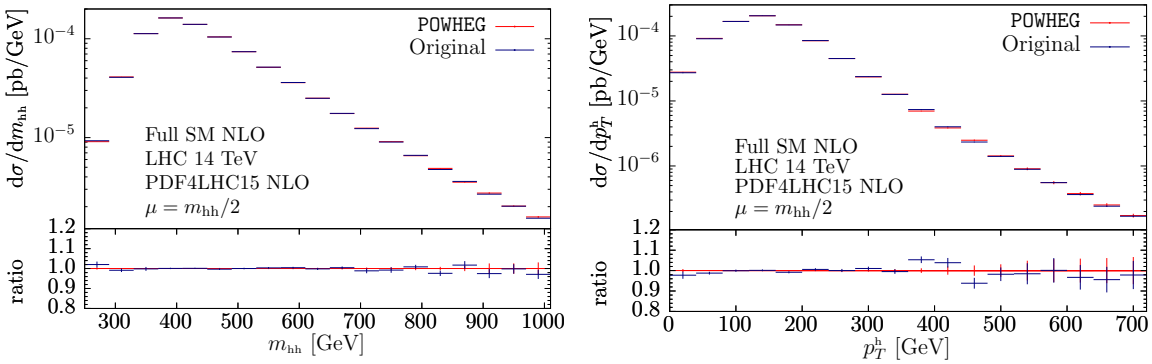

Figure 2. The $m_{\rm hh}$ and $p_T^{\rm h}$ distributions calculated from the grid versus the full calculation.

3.1 Comparison with previous NLO results

A very strong consistency check of the new implementation, which allows to test at the same time the real amplitudes and their stability, the implementation of the grid for the virtual two-loop amplitude and all the various parts of the code relevant for the NLO fixed order computation is a comparison with the previous NLO results computed in refs. [21, 23]. A comparison at the level of individual phase space points shows that the grid interpolation slightly increases the numerical uncertainty associated to the virtual amplitude results, which were calculated with percent level precision in the previous publications. At the level of differential distributions we found excellent agreement, not only for the full NLO results, but also for the various other approximations available and for uncertainties related to scales variation.

In figure 2 we show a comparison between the NLO predictions obtained with the `POWHEG-BOX` generator and the original ones from ref. [23]. In the `MG5_aMC@NLO` case, where only showered results are available, we made a similar validation plot for the $m_{\rm hh}$ distribution, as it is insensitive to shower effects.

We should mention at this point that beyond $p_T^{\rm h} \sim 650\,\text{GeV}$, a systematic bias stemming from lack of statistics in the grid starts to develop. As a consequence, the results obtained with the grid will be systematically below the "true" results. The difference is within the statistical uncertainty up to about $p_T^{\rm h} \sim 750\,\text{GeV}$, and increases to about 20% at $p_T^{\rm h} \sim 1\,\text{TeV}$ (and $m_{\rm hh} \sim 2\,\text{TeV}$).

3.2 Comparisons at the level of Les Houches event files

Before presenting results for NLO predictions matched to the parton shower, we show comparisons of NLO curves with results at the Les Houches event (LHE) level, after the first hard emission is weighted with the Sudakov factor according to the `POWHEG` method. Even though the LHE level predictions still need to be showered, such a comparison allows to test the implementation and, once the results are fully showered, to disentangle the impact of the shower from the one due to the `POWHEG` exponentiation. For observables which are inclusive in the extra radiation, the fixed order NLO and LHE level predictions should be in perfect agreement. We show the level of agreement between the NLO and LHE curves

JHEP08(2017)088

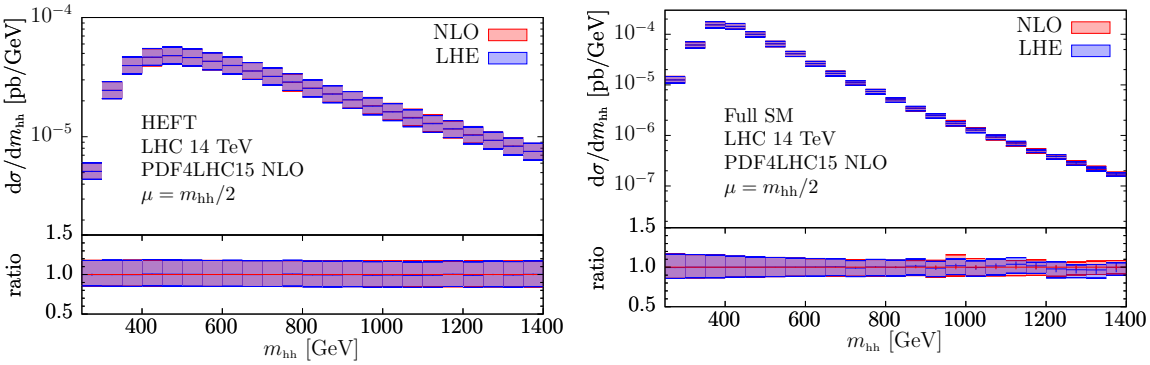

(a) $m_{\rm hh}$ in HEFT (b) $m_{\rm hh}$ in the full SM

Figure 3. Higgs-pair invariant mass distributions $m_{\rm hh}$ in the HEFT approximation and in the full SM at fixed NLO level compared to LHE level, where in the latter the value `hdamp` $= \infty$ has been used.

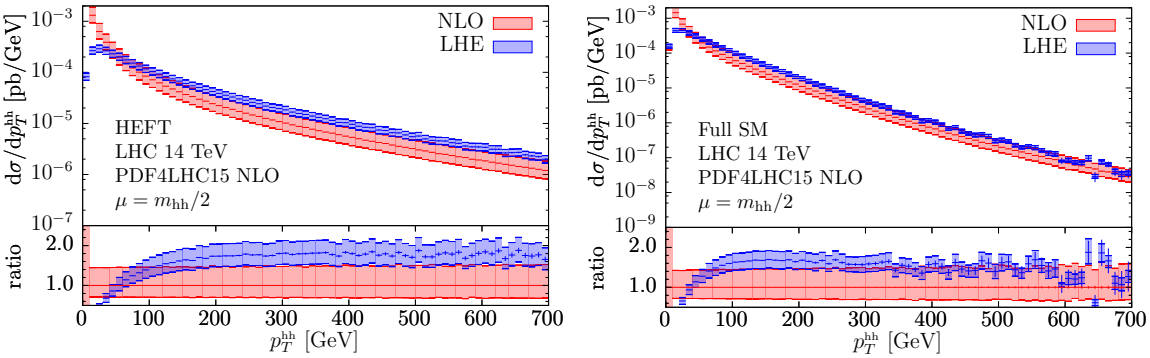

(a) $p_T^{\rm hh}$ in HEFT (b) $p_T^{\rm hh}$ in the full SM

Figure 4. Higgs-pair transverse momentum distributions $p_T^{\rm hh}$ in the HEFT approximation and in the full SM at fixed NLO level compared to LHE level (with `hdamp` $= \infty$).

for the Higgs-boson pair invariant mass m_{hh} in figure 3, where a comparison is shown for predictions in the HEFT approximation and the full SM. For observables which are directly sensitive to soft gluon radiation, like the $p_T^{\rm hh}$ distribution in the limit $p_T^{\rm hh} \to 0$, one instead expects to observe Sudakov suppression in the soft region. This can be seen in figure 4, where we can clearly see the suppression in the region where the fixed order NLO results become unreliable. We also note that the LHE predictions are enhanced in the high transverse momentum region compared to the NLO curve. This is due to subleading contributions in the exponential, which in the case of large radiative corrections can become sizable, in particular for observables like $p_T^{\rm hh}$, where NLO is the first non-trivial order to describe the distribution. Analogous effects have already been observed in several other similar processes with large K-factors [103–106], and we refer the interested reader to refs. [103, 104] for more details. We have explored the possibility to limit the amount of hard radiation which is exponentiated by changing the `hdamp` parameter in `POWHEG`. We recall that this allows to divide the contributions of the real radiation R which are exponentiated in the Sudakov

JHEP08(2017)088

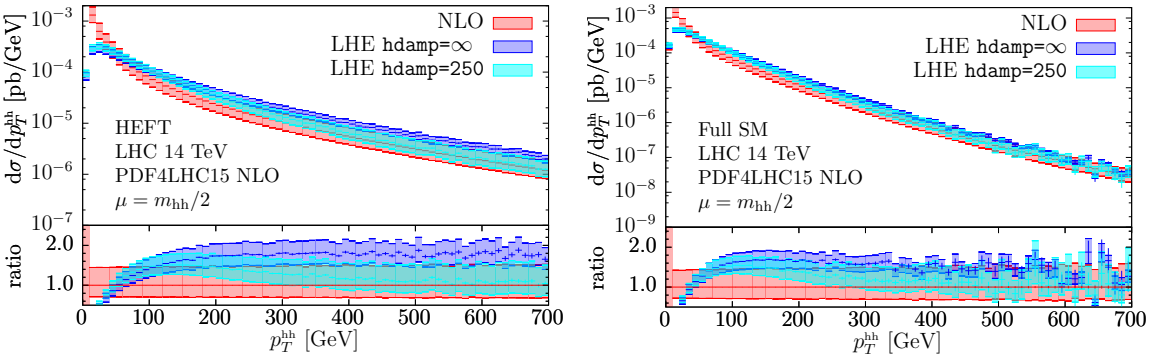

(a) $p_T^{\rm hh}$ in basic HEFT

(b) $p_T^{\rm hh}$ in the full SM

Figure 5. Comparison of the POWHEG predictions with hdamp $= \infty$ at LHE level with predictions in which we set hdamp $= 250$; for HEFT (left) and with full top-quark mass dependence (right).

factor into a singular part $R_{\rm sing}$ and a regular part $R_{\rm reg}$, as follows:

$$R_{\rm sing} = R \times F\,, \tag{3.1}$$

$$R_{\rm reg} = R \times (1 - F)\,, \tag{3.2}$$

where the transition function F is chosen to be

$$F = \frac{h^2}{(p_T^{\rm hh})^2 + h^2}\,. \tag{3.3}$$

In figure 5 we compare the default POWHEG setting, $h =$ hdamp $= \infty$, with predictions where we use hdamp $= 250\,$GeV. The left plot shows predictions in the HEFT, whereas on the right we show results in the full SM. We observe that in both cases above 500 GeV the LHE curve with hdamp $= 250\,$GeV reproduces the NLO results as expected. It is interesting to study how this additional source of theoretical uncertainty is affecting other observables, especially those for which our predictions are NLO accurate. To understand this better, in figure 6 we show a similar comparison for $m_{\rm hh}$ (left) and the transverse momentum of a (randomly chosen) Higgs boson $p_T^{\rm h}$ (right), with full top quark mass dependence. The $m_{\rm hh}$ observable is completely insensitive to additional radiation, and for this reason it is unaffected by a modification of the hdamp factor. This is not true for $p_T^{\rm h}$, which is sensitive to the recoil against additional jet activity. For this reason we observe deviations between the NLO predictions and the LHE-level curves, the latter becoming slightly larger for harder transverse momenta. The predictions for hdamp $= 250$ are in general closer to the NLO ones over the whole kinematical range of $p_T^{\rm h}$. We stress however that, contrary to $p_T^{\rm hh}$, where the differences between the predictions for hdamp $= \infty$ and the one for hdamp $= 250\,$GeV reach 80% above 500 GeV, for $p_T^{\rm h}$ the differences are at the 10–15% level, i.e. well within the scale uncertainties.

Since the uncertainty related to the value for hdamp is very tightly related to the POWHEG way of matching NLO to the parton-shower, it is important to compare these predictions with other matching schemes. We will comment more on this aspect in section 3.4, where we compare NLO+PS predictions obtained with POWHEG and MG5_aMC@NLO.

JHEP08(2017)088

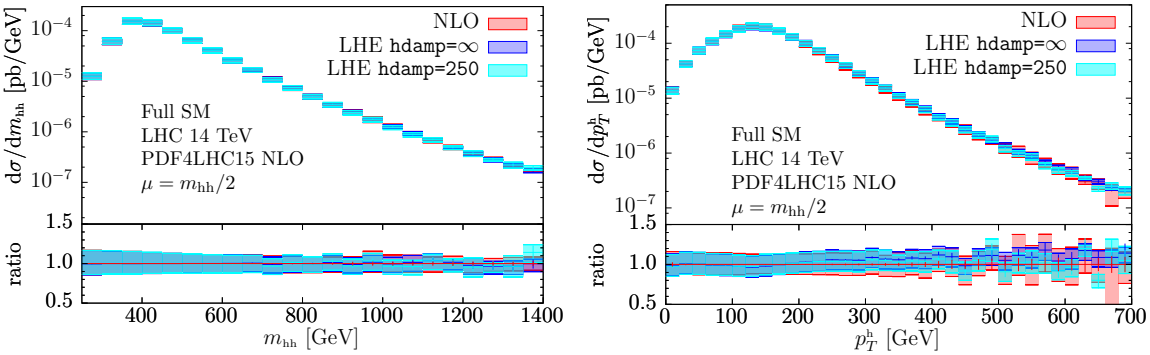

(a) $m_{\rm hh}$ in the full SM

(b) $p_T^{\rm h}$ in the full SM

Figure 6. Comparison of the POWHEG predictions with hdamp $= \infty$ at LHE level with predictions in which we set hdamp $= 250$, for the Higgs-pair invariant mass $m_{\rm hh}$ (left) and the transverse momentum of any (randomly chosen) Higgs boson. The predictions are computed with full top-quark mass dependence.

3.3 Discussion of NNLO effects

We mentioned in the previous section that the enhancement in the tail of $p_T^{\rm hh}$ in the prediction at the LHE-level is due to subleading contributions in the Sudakov factor, which are intrinsically taken into account in the matching à la POWHEG. As already pointed out and discussed in [103], it is therefore interesting to compare NLO+PS predictions obtained with POWHEG to the full NNLO predictions, if they are available. This is indeed the case if we restrict ourselves to results in the basic HEFT, for which differential NNLO results were computed in ref. [18].[1] The comparison is of course meaningful only for those observables which are LO accurate in our NLO calculation and which therefore are not sensitive to the additional two-loop virtual corrections included in the HEFT NNLO predictions. In figure 7 we consider again the transverse momentum of the Higgs boson pair and compare the NNLO results with two different LHE-level predictions from POWHEG. On the left we keep the default setting in which hdamp $= \infty$, on the right we set hdamp $= 250\,$GeV. In the former plot we observe a good agreement of the LHE-level curve with hdamp $= \infty$ with the NNLO predictions in the transverse momentum range between 200 GeV and 400 GeV. While the LHE-level result flattens out around 250 GeV, the NNLO result decreases slightly for larger $p_T^{\rm hh}$. The two theory uncertainty bands due to scale variation however largely overlap. The plot on the right shows instead that, by limiting the amount of real radiation in the Sudakov factor, the LHE-level prediction falls onto the NLO result at high p_T, and therefore cannot reproduce the NNLO behaviour.

As a further step, we can assess the impact of the parton shower, by analyzing the same observable with NLO+PS predictions showered with Pythia 8. Figure 8 shows an analogous comparison, where the NLO curves with and without shower are plotted against the NNLO predictions. We observe that the shower has a large effect on the tail of the $p_T^{\rm hh}$ distribution, such that the NNLO curve lies between the NLO+PS and the NLO fixed order

[1] We are grateful to Javier Mazzitelli for providing us the NNLO predictions shown in the comparisons of this section.

JHEP08(2017)088

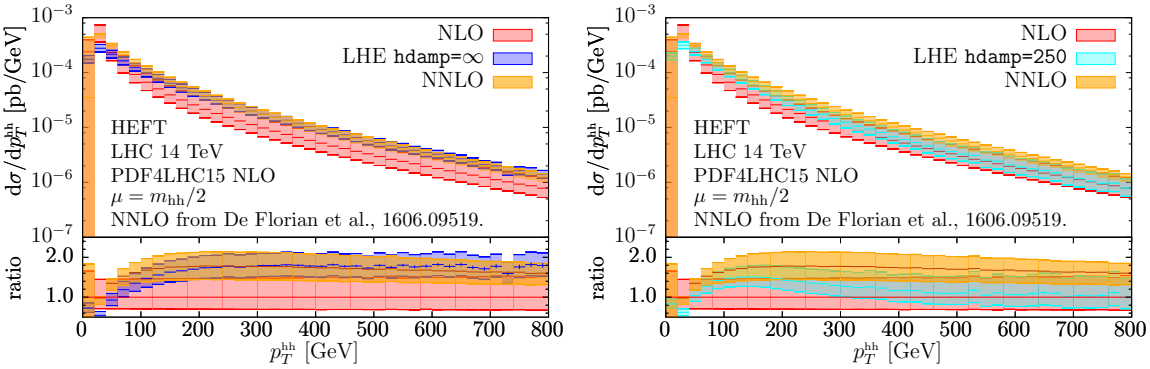

(a) $p_T^{\rm hh}$ in basic HEFT, default value for `hdamp`.

(b) $p_T^{\rm hh}$ in basic HEFT, `hdamp` = 250.

Figure 7. Comparison of the NNLO results from ref. [18] with default `POWHEG` predictions (`hdamp` = ∞) at LHE level (left) and predictions in which we set `hdamp` = 250 (right) for the Higgs-pair transverse momentum $p_T^{\rm hh}$.

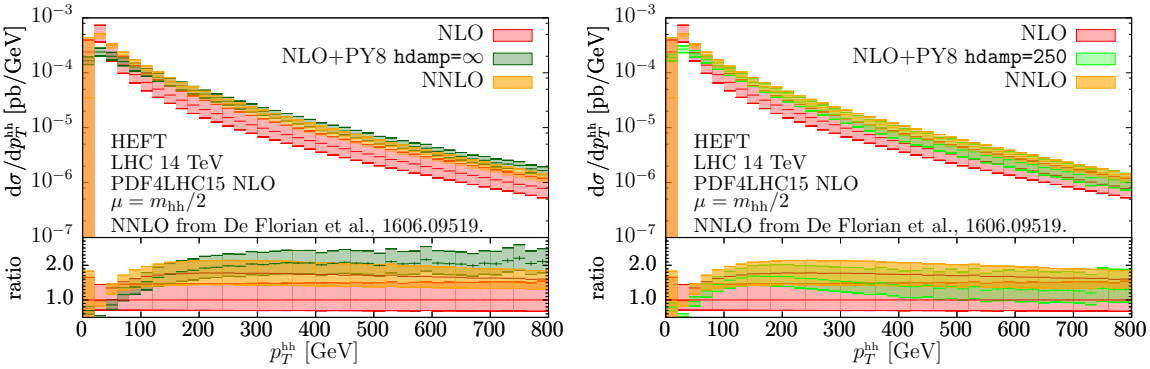

Figure 8. Comparison of the NNLO results from ref. [18] with default `POWHEG` predictions (`hdamp` = ∞) at NLO+PS level (left) and predictions in which we set `hdamp` = 250 (right) for the Higgs-pair transverse momentum $p_T^{\rm hh}$. `Pythia 8` was used to shower the events.

curve for `hdamp` = ∞. On the other hand, for `hdamp` = 250 GeV, the NLO+PS result by construction is closer to the NLO fixed order result. We should point out however that these considerations within the basic HEFT approximation may not carry over analogously to the full calculation (where NNLO predictions are not available), because it is well known that the HEFT approximation does not have the correct scaling behaviour at large transverse momenta.

3.4 NLO plus parton shower matched results

We now compare fixed order NLO results to our default `POWHEG` results, where we use `hdamp=250` and the `Pythia 8` shower. In figure 9 we show the Higgs boson pair invariant mass distribution and the transverse momentum distribution of a randomly chosen Higgs boson for both the fixed order and the showered calculation. As is to be expected, the invariant mass distribution is rather insensitive to the parton shower. In figure 10 the p_T-distributions of the harder and softer Higgs boson are shown.

JHEP08(2017)088

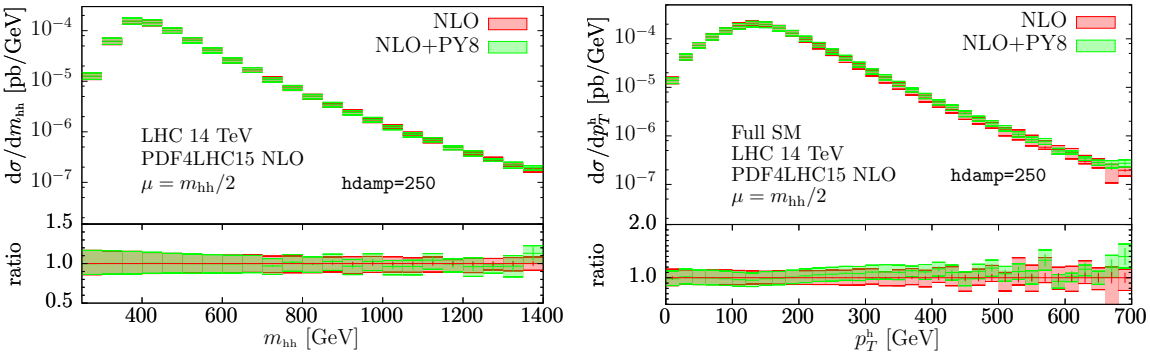

Figure 9. Higgs boson pair invariant mass distribution m_{hh} and transverse momentum distribution of a (randomly chosen) Higgs boson at $\sqrt{s} = 14\,\text{TeV}$, comparing the fixed order result with showered results from the POWHEG-BOX.

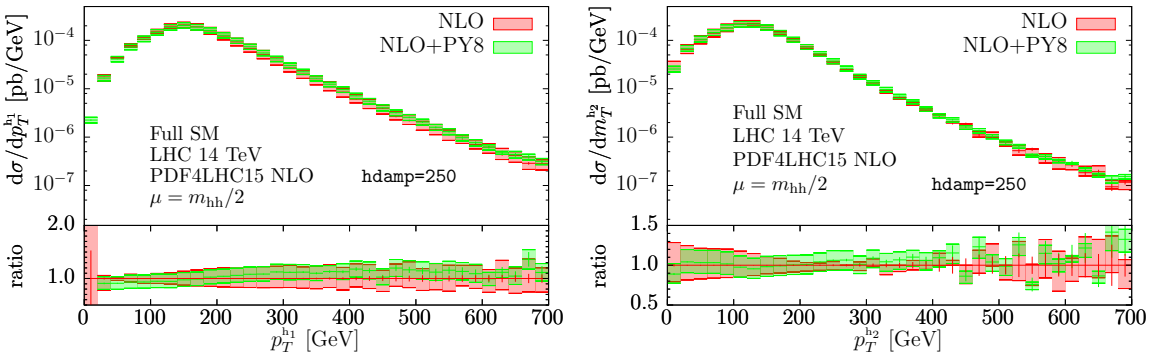

Figure 10. Transverse momentum distribution of the leading ($p_T^{\rm h_1}$) and subleading ($p_T^{\rm h_2}$) Higgs boson, comparing fixed order and showered results. The first bin in $p_T^{\rm h_1}$ in the fixed order NLO calculation is negative and therefore does not appear in the upper part of the plot.

We should mention at this point that the distributions of the "harder" ($p_T^{\rm h_1}$) and "softer" ($p_T^{\rm h_2}$) Higgs boson, calculated at fixed (NLO) order, are somewhat infrared sensitive if no cuts are placed on the Higgs boson transverse momenta. The reason is that, if the transverse momenta $p_T^{\rm h_1}$ and $p_T^{\rm h_2}$ are very close to each other, the available phase space for the extra radiation in the real corrections is severely restricted, leading to large logarithms which are not sufficiently balanced by the $2 \to 2$ contributions. To illustrate this fact, we consider the total cross section as a function of Δ, with the kinematic requirements $p_T^{\rm h_1} \geq \Delta$, $p_T^{\rm h_2} \geq 0$. The cross section shows an unphysical behaviour as $\Delta \to 0$, see figure 11: the total cross section as a function of Δ peaks around $\Delta = 14\,\text{GeV}$ and then decreases for smaller values of Δ, even though the available phase space for $p_T^{\rm h_1}$ is larger. This behaviour is an artifact of the fixed order calculation and is the reason why "symmetric cuts" (i.e. the same $p_{T,\rm min}$ values for both final state particles in a $2 \to 2$ calculation at NLO) should be avoided. For a more detailed discussion of this point we refer to refs. [107–109]. Here we only note that this is the reason why, with "symmetric" cuts $p_{T,\rm min}^{\rm h_1} = p_{T,\rm min}^{\rm h_2} = 0$ and fine binning, the first bin(s) of the $p_T^{\rm h_1}$ distribution are negative at fixed order, while this behaviour is cured by the Sudakov factor, so it is absent in the LHE level and showered results.

JHEP08(2017)088

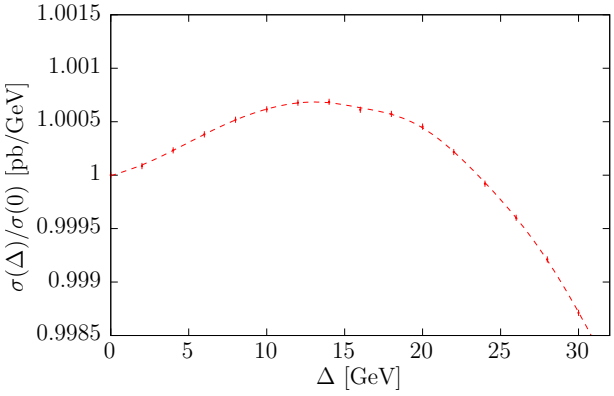

Figure 11. Total cross section as a function of the difference Δ between the $p_{T,\min}$ cut placed on the harder and the softer Higgs boson transverse momenta.

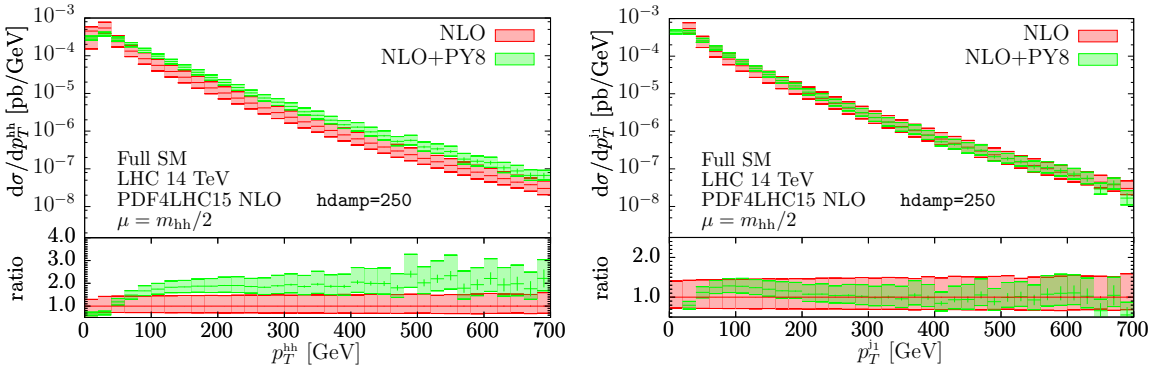

Figure 12. Higgs boson pair transverse momentum distribution $p_T^{\rm hh}$ (left) and leading jet transverse momentum distribution $p_T^{\rm j_1}$ (right), comparing fixed order and showered results.

Figure 12 displays the transverse momentum distributions of the Higgs boson pair and of the (leading) jet. As discussed already in the context of figure 5, the $p_T^{\rm hh}$ distribution diverges at fixed order for $p_T^{\rm hh} \to 0$, while the showered result is able to provide reliable predictions in the low $p_T^{\rm hh}$ region. We notice that the scale variation band is reduced in the showered result compared to the fixed order calculation. The scale uncertainties on the fixed order results are particularly large for these distributions as they are — except for the first bin — determined by the $2 \to 3$ kinematics, which is described only at leading order accuracy by our calculation.

In figure 13 we show the difference in azimuthal angle, $\Delta\Phi^{hh}$, and the radial separation, $\Delta R^{\rm hh} = \sqrt{(\eta_1 - \eta_2)^2 + (\Phi_1 - \Phi_2)^2}$, of the two Higgs bosons. We see that the unphysical behaviour for $\Delta\Phi^{hh} \to 0$ of the fixed order result is cured by the Sudakov form factor, and again the scale uncertainties of the fixed order calculation are relatively large because the tail of the distribution is predicted at the first non-trivial order. In the $\Delta R^{\rm hh}$ distribution, we observe that the shower populates the region $\Delta R^{\rm hh} < \pi$, which at fixed order is given by the $2 \to 3$ component only.

Figure 14 compares the predictions obtained with the `Pythia6` shower to the `Pythia8` results both in the basic HEFT approximation and in the full SM. It is instructive to make

JHEP08(2017)088

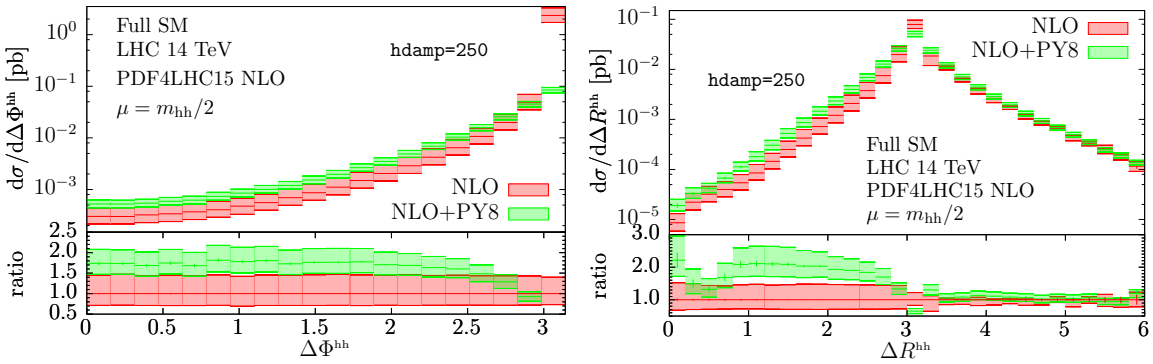

Figure 13. Azimuthal angle separation $\Delta\Phi^{\rm hh}$ (left) and radial separation $\Delta R^{\rm hh}$ (right) of the two Higgs bosons, comparing fixed order and showered results.

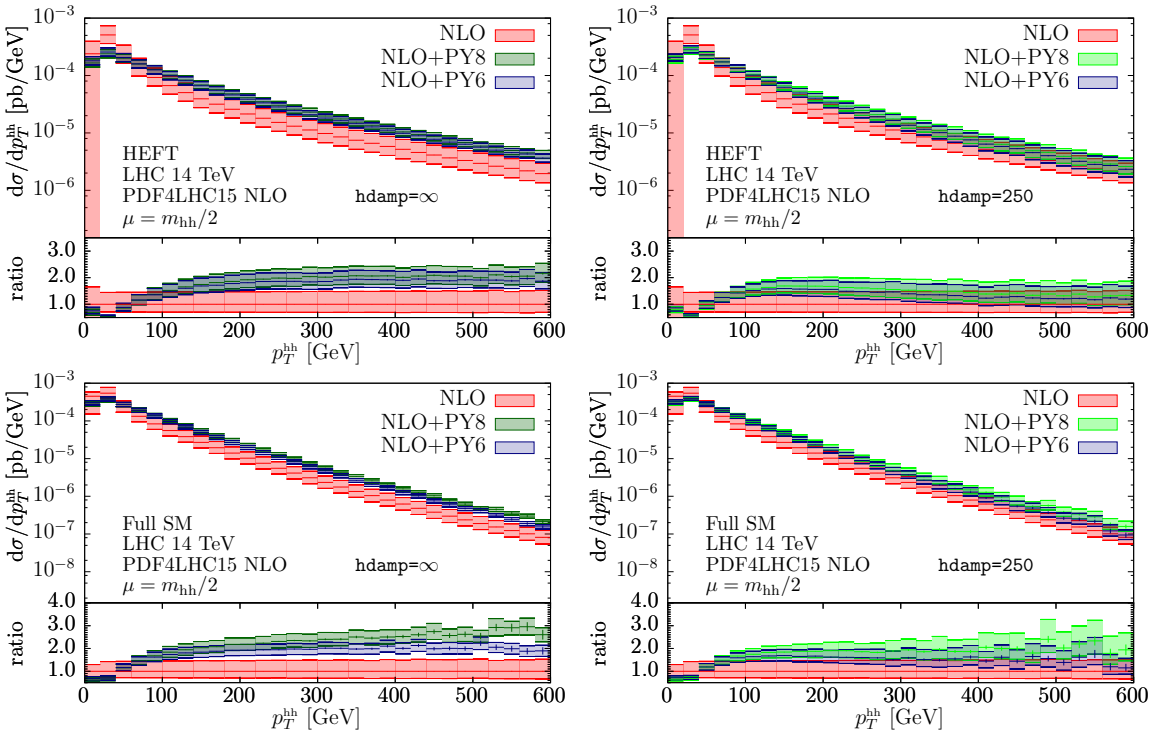

Figure 14. Higgs boson pair transverse momentum distribution $p_T^{\rm hh}$ (left column with `hdamp=`∞, right column with `hdamp=250`) comparing the fixed order result with showered results from both `Pythia 6` and `Pythia 8` in the basic HEFT approximation (upper row) and in the full SM (lower row).

this comparison for `hdamp=`∞ (left column) as well as for `hdamp=250` (right column). In the basic HEFT approximation the differences between `Pythia 6` and `Pythia 8` are small, and setting `hdamp` to a finite value restores the agreement between the NLO and the NLO+PS curves at large transverse momentum. The latter is also true in the full SM. However, in the full SM, the difference between `Pythia 6` and `Pythia 8` is much larger, `Pythia 8` showing a considerably harder spectrum in the tail of the $p_T^{\rm hh}$ distribution.

JHEP08(2017)088

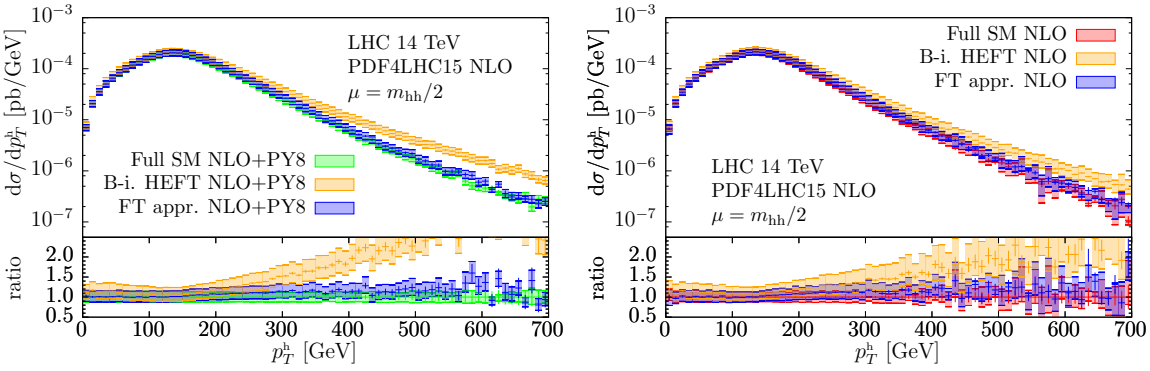

(a) Showered results (`hdamp=250`). (b) Fixed order results.

Figure 15. p_T^h distribution comparing (a) showered results based on matrix elements in various approximations (full, $\mathrm{FT}_{\mathrm{approx}}$, Born-improved HEFT) with (b) fixed order results.

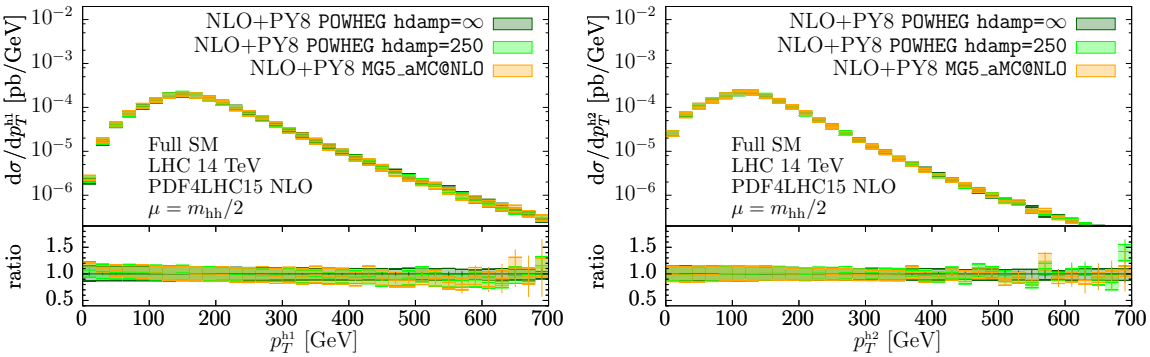

Figure 16. Leading and subleading Higgs boson transverse momentum distributions $p_T^{\mathrm{h}_1}$ and $p_T^{\mathrm{h}_2}$, comparing showered results with `POWHEG` and `MG5_aMC@NLO`.

To conclude this section, in figure 15a we compare the full results with calculations where the underlying matrix elements are based on two approximations, either $\mathrm{FT}_{\mathrm{approx}}$ or Born-improved HEFT. All matrix elements are combined with the same `Pythia 8` shower. In order to assess the effect of the parton shower on the various approximations, we also show the fixed order results in figure 15b. The broad features of these approximations remain unchanged after showering, however, as the showered results have smaller scale uncertainties, the differences between these approximations are actually enhanced if a parton shower is attached.

3.4.1 Comparison between `POWHEG` and `MG5_aMC@NLO`

In this section we compare the `POWHEG` results with results from `MG5_aMC@NLO`, the latter being based on the same grid in the invariants $\hat{s}$ and $\hat{t}$ for the virtual two-loop corrections as the `POWHEG` results, and based on the same `Pythia 8` shower. Therefore the differences between the results can be attributed to differences in the matching scheme.

In figures 16 to 18 we show `POWHEG` results for two different values of `hdamp` compared to `MG5_aMC@NLO` results. While for the $p_T^{\mathrm{h}_1}$ and $p_T^{\mathrm{h}_2}$ distributions the differences are mostly small, they are, as to be expected, more pronounced for the distributions where the shower populates

JHEP08(2017)088

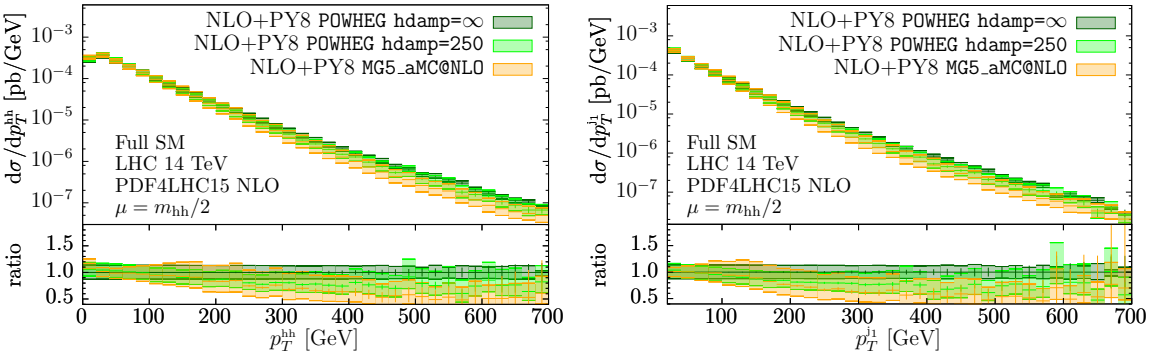

Figure 17. Higgs boson pair transverse momentum distribution $p_T^{\rm hh}$ (left) and $p_T^{\rm j_1}$ distribution (right), comparing showered results with POWHEG and MG5_aMC@NLO. For the $p_T^{\rm j_1}$ distribution we used a cut of $p_{T,\rm min}^{\rm jet} = 20\,\text{GeV}$.

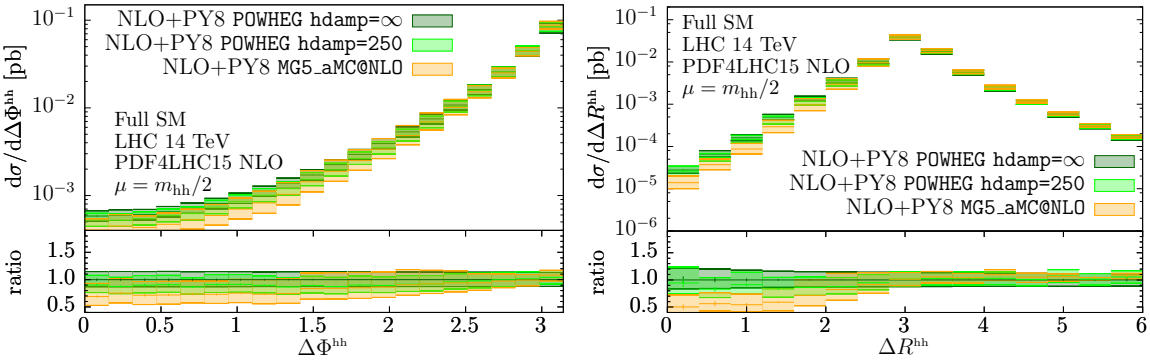

Figure 18. Azimuthal angle separation $\Delta\Phi^{\rm hh}$ (left) and separation $\Delta R^{\rm hh}$ (right).

kinematic regions which are predicted at the first non-trivial order by the NLO fixed order calculation. Focusing on the comparison between the POWHEG curve with hdamp=250, which is our default, we can say that in general the two predictions agree well within the scale and statistical uncertainties. The small $\Delta R^{\rm hh}$ region, on the right of figure 18, shows the largest differences, which is not surprising as it is dominated by (multi-)jet events. We should also mention that the curve for hdamp=250 in these figures is close to the NLO curves by construction, as can be seen by comparing to the fixed order results shown in the previous subsection.

In figure 19 we vary the shower starting scale Q_{sh} in MG5_aMC@NLO by a factor of two around the default value. In the latest version of MG5_aMC@NLO (version 2.5.3 onwards), the shower starting scale is picked with some probability distribution to be in the interval shower_scale_factor $\times[0.1\,H_T/2, H_T/2]$ with H_T computed with Born kinematics, therefore to perform the scale variation we set the shower_scale_factor in the run card to 0.5, 1 and 2.

The $m_{\rm hh}$ distribution can be considered as a control plot to demonstrate that, as expected, this has no effect on the $m_{\rm hh}$ distribution. In contrast, in the $p_T^{\rm hh}$ distribution, the differences due to variations of the matching scale start to exceed the scale uncertainties towards larger $p_T^{\rm hh}$ values.

JHEP08(2017)088

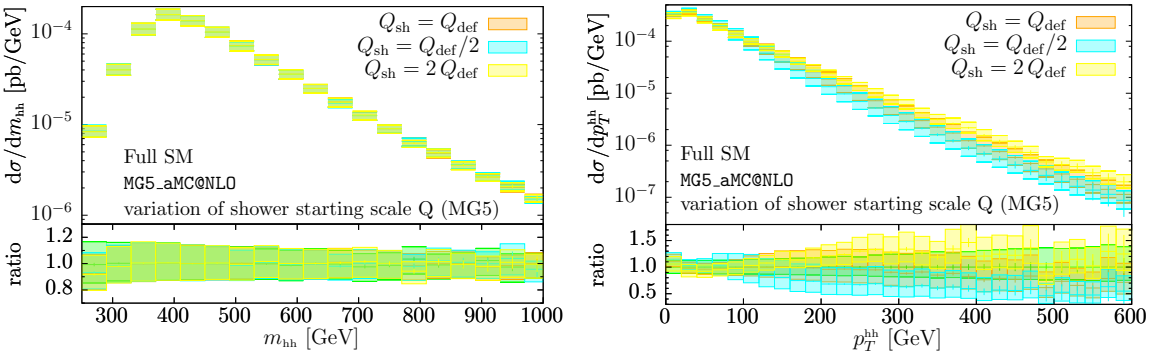

Figure 19. m_{hh} and p_T^{hh} distributions comparing showered results based on the same matrix elements (NLO with full top quark mass dependence), varying the shower starting scale Q_{sh} in `MG5_aMC@NLO` by a factor of two up and down. The ratio plot is normalized to the `POWHEG` result for `hdamp=250`. The bands show the envelope of the variation of the renormalisation and factorisation scales.

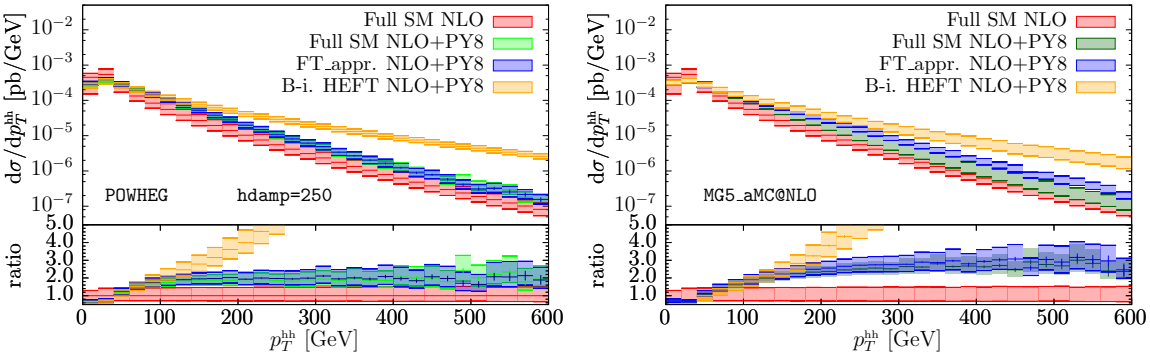

Figure 20. Higgs boson pair transverse momentum distribution p_T^{hh} comparing fixed order and showered results. Left panel: `POWHEG`, right panel: `MG5_aMC@NLO`.

Because of the fact that for the p_T^{hh} distribution, the tail is predicted at the first non-trivial order, the effect of the shower on this distribution is rather large, exceeding a factor of two beyond $p_T^{\mathrm{hh}} \sim 300\,\mathrm{GeV}$, as shown in figure 20. However, as can also be seen from figure 20, the differences due to the shower are still much smaller than the difference between the full calculation and the Born-improved HEFT approximation, which is off by an order of magnitude for $p_T^{\mathrm{hh}} > 500\,\mathrm{GeV}$. Figure 20 also shows that $\mathrm{FT}_{\mathrm{approx}}$ does a good job for this observable, as the tail of the p_T^{hh} distribution is determined by the real radiation. In the `POWHEG` case, the $\mathrm{FT}_{\mathrm{approx}}$ curve still lies above the full result because the differences in the virtual part enter the $\bar{B}$ function in `POWHEG`, which determines the overall normalisation for the shower.

Finally, we compare in figure 21 the fixed order result to showered results using different values for `hdamp` in `POWHEG` and for the shower starting scale Q_{sh} in `MG5_aMC@NLO`. The new shower starting scale in `MG5_aMC@NLO` is picked in some interval with $H_T/2$ as its maximum as stated above, while the old shower starting scale was picked in the interval $[0.1\sqrt{\hat{s}}, \sqrt{\hat{s}}]$. One can observe that with the new shower starting scale in `MG5_aMC@NLO`, $Q_{\mathrm{sh}} = Q_{\mathrm{def}}^{\mathrm{new}}$, the

JHEP08(2017)088

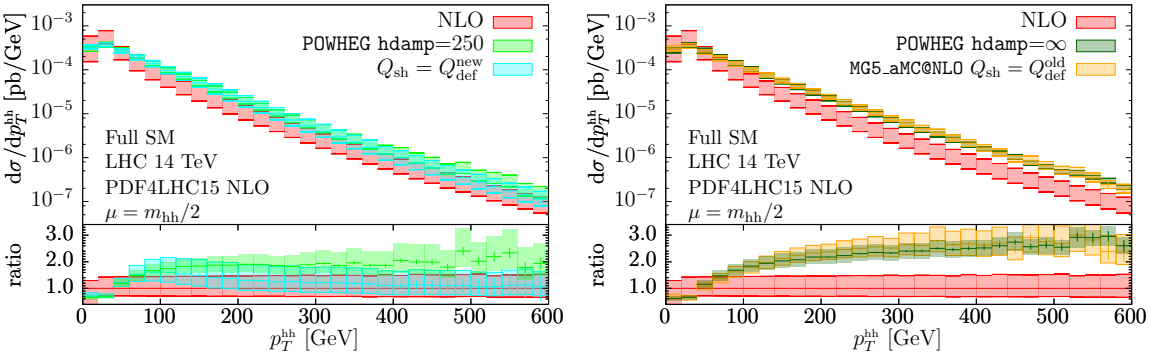

Figure 21. $p_T^{\rm hh}$ distribution comparing showered results with different values for `hdamp` in `POWHEG` resp. the shower starting scale $Q_{\rm sh}$ in `MG5_aMC@NLO` compared to the fixed order result.

showered results match onto the fixed order curve at large values of $p_T^{\rm hh}$, while the latter is not the case for `POWHEG` with `hdamp=`∞ and `MG5_aMC@NLO` with the old default shower starting scale.

4 Conclusions

We have presented the combination of the full NLO prediction for Higgs boson pair production, including the top quark mass dependence at two loops, with a parton shower. This has been implemented within two frameworks, `POWHEG-BOX` and `MG5_aMC@NLO`, using the same `Pythia 8.2` shower in both cases. Individual phase-space points of the two-loop amplitude, which depends only on the two independent kinematic invariants $\hat{s}$ and $\hat{t}$ once the top-quark and Higgs boson masses are fixed, have been used to create a grid and combined with an interpolation framework, such that a value for the amplitude can be obtained at any phase space point without re-evaluating the loop integrals.

We find that the impact of the parton shower on the transverse momentum distribution of one Higgs boson, $p_T^{\rm h}$, is quite small and that the features of the various approximations that have appeared previously in the literature are preserved by the shower.

The impact of the shower on the $p_T^{\rm hh}$, $\Delta\Phi^{hh}$ and ΔR^{hh} distributions is fairly large, as these are the distributions where the tail is predicted at the first non-trivial order in the fixed order calculation. In the tail of the $p_T^{\rm hh}$ distribution, around $p_T^{\rm hh} \sim 400\,\text{GeV}$, the showered NLO results are larger than the fixed order results by more than a factor of two, within both `POWHEG` and `MG5_aMC@NLO`. This feature is also present if `Pythia 6` is used instead of `Pythia 8`, and if we vary the shower starting scale in `MG5_aMC@NLO`. However, the differences due to the shower in the $p_T^{\rm hh}$ distribution are still much smaller than the discrepancy between the showered full calculation and the showered Born-improved HEFT approximation, the latter overshooting the full result by an order of magnitude around $p_T^{\rm hh} \sim 400\,\text{GeV}$, worsening towards higher $p_T^{\rm hh}$ values. As expected, the $\text{FT}_{\text{approx}}$ results, which include the full mass dependence in the real radiation, behave very similar to the full calculation in the (real radiation dominated) tails of the distributions like $p_T^{\rm hh}$.

JHEP08(2017)088

In summary, we observe that the inclusion of the full mass dependence in general has a more important impact on the distributions relevant to Higgs boson pair production than effects coming from different shower matching schemes, variations of the shower starting scales, different parton showers or different PDFs. A detailed study of hadronisation effects and Higgs boson decays will be performed in a subsequent publication.

The `POWHEG` version of the code for Higgs boson pair production developed for this work is publicly available in the `POWHEG-BOX V2` package, under the `User-Processes-V2/ggHH/` directory, and will become available also in the newer `POWHEG-BOX RES` version in the `User-Processes-RES/ggHH/` folder. All the information can be found at the web page `http://powhegbox.mib.infn.it`. The implementation in `MG5_aMC@NLO` is not part of the public release yet, but the customised code can be obtained by contacting the authors.

We hope that making two-loop results available in the form of a grid included in public Monte Carlo programs, as done in this work, will open the door to further developments in this direction.

Acknowledgments

We would like to thank our collaborators Sophia Borowka, Nicolas Greiner, Johannes Schlenk and Tom Zirke for their contribution to the double Higgs fixed order NLO project and Simone Alioli for interesting discussions and suggestions concerning the `POWHEG-BOX`. We also thank Javier Mazzitelli for providing us the NNLO HEFT data for comparisons. We also would like to thank Fabio Maltoni and Paolo Torrielli for useful discussions and Carlo Oleari for comments on the manuscript. G.L. thanks the Max Planck Institute for Physics for hospitality during several phases of this work. This research was supported in part by the Research Executive Agency (REA) of the European Union under the Grant Agreement PITN-GA2012316704 (HiggsTools). E.V. acknowledges support from the Netherlands Foundation for Fundamental Research of Matter (FOM) under project number 15PR3224. We gratefully acknowledge support and resources provided by the Max Planck Computing and Data Facility (MPCDF).

References

[1] CMS collaboration, *Search for Higgs boson pair production in the final state containing two photons and two bottom quarks in proton-proton collisions at* $\sqrt{s} = 13$ *TeV*, CMS-PAS-HIG-17-008 (2017).

[2] ATLAS collaboration, *Search for pair production of Higgs bosons in the* $b\bar{b}b\bar{b}$ *final state using proton-proton collisions at* $\sqrt{s} = 13$ *TeV with the ATLAS detector*, ATLAS-CONF-2016-049 (2016).

JHEP08(2017)088

[3] CMS collaboration, *Search for pair production of Higgs bosons in the two tau leptons and two bottom quarks final state using proton-proton collisions at* $\sqrt{s} = 13$ *TeV*, CMS-PAS-HIG-17-002 (2017).

[4] ATLAS collaboration, *Searches for Higgs boson pair production in the* $hh \to bb\tau\tau, \gamma\gamma WW^*, \gamma\gamma bb, bbbb$ *channels with the ATLAS detector*, *Phys. Rev.* **D 92** (2015) 092004 [arXiv:1509.04670] [INSPIRE].

[5] CMS collaboration, *Search for resonant and non-resonant Higgs boson pair production in the* $b\bar{b}l\nu l\nu$ *final state at* $\sqrt{s} = 13$ *TeV*, CMS-PAS-HIG-17-006 (2017).

[6] O.J.P. Eboli, G.C. Marques, S.F. Novaes and A.A. Natale, *Twin Higgs boson production*, *Phys. Lett.* **B 197** (1987) 269 [INSPIRE].

[7] E.W.N. Glover and J.J. van der Bij, *Higgs boson pair production via gluon fusion*, *Nucl. Phys.* **B 309** (1988) 282 [INSPIRE].

[8] T. Plehn, M. Spira and P.M. Zerwas, *Pair production of neutral Higgs particles in gluon-gluon collisions*, *Nucl. Phys.* **B 479** (1996) 46 [*Erratum ibid.* **B 531** (1998) 655] [hep-ph/9603205] [INSPIRE].

[9] S. Dawson, S. Dittmaier and M. Spira, *Neutral Higgs boson pair production at hadron colliders: QCD corrections*, *Phys. Rev.* **D 58** (1998) 115012 [hep-ph/9805244] [INSPIRE].

[10] R. Frederix et al., *Higgs pair production at the LHC with NLO and parton-shower effects*, *Phys. Lett.* **B 732** (2014) 142 [arXiv:1401.7340] [INSPIRE].

[11] F. Maltoni, E. Vryonidou and M. Zaro, *Top-quark mass effects in double and triple Higgs production in gluon-gluon fusion at NLO*, *JHEP* **11** (2014) 079 [arXiv:1408.6542] [INSPIRE].

[12] J. Grigo, J. Hoff, K. Melnikov and M. Steinhauser, *On the Higgs boson pair production at the LHC*, *Nucl. Phys.* **B 875** (2013) 1 [arXiv:1305.7340] [INSPIRE].

[13] J. Grigo, K. Melnikov and M. Steinhauser, *Virtual corrections to Higgs boson pair production in the large top quark mass limit*, *Nucl. Phys.* **B 888** (2014) 17 [arXiv:1408.2422] [INSPIRE].

[14] J. Grigo, J. Hoff and M. Steinhauser, *Higgs boson pair production: top quark mass effects at NLO and NNLO*, *Nucl. Phys.* **B 900** (2015) 412 [arXiv:1508.00909] [INSPIRE].

[15] G. Degrassi, P.P. Giardino and R. Gröber, *On the two-loop virtual QCD corrections to Higgs boson pair production in the standard model*, *Eur. Phys. J.* **C 76** (2016) 411 [arXiv:1603.00385] [INSPIRE].

[16] D. de Florian and J. Mazzitelli, *Two-loop virtual corrections to Higgs pair production*, *Phys. Lett.* **B 724** (2013) 306 [arXiv:1305.5206] [INSPIRE].

[17] D. de Florian and J. Mazzitelli, *Higgs boson pair production at next-to-next-to-leading order in QCD*, *Phys. Rev. Lett.* **111** (2013) 201801 [arXiv:1309.6594] [INSPIRE].

[18] D. de Florian et al., *Differential Higgs boson pair production at next-to-next-to-leading order in QCD*, *JHEP* **09** (2016) 151 [arXiv:1606.09519] [INSPIRE].

[19] D.Y. Shao, C.S. Li, H.T. Li and J. Wang, *Threshold resummation effects in Higgs boson pair production at the LHC*, *JHEP* **07** (2013) 169 [arXiv:1301.1245] [INSPIRE].

[20] D. de Florian and J. Mazzitelli, *Higgs pair production at next-to-next-to-leading logarithmic accuracy at the LHC*, *JHEP* **09** (2015) 053 [arXiv:1505.07122] [INSPIRE].

JHEP08(2017)088

[21] S. Borowka et al., *Higgs boson pair production in gluon fusion at next-to-leading order with full top-quark mass dependence*, *Phys. Rev. Lett.* **117** (2016) 012001 [*Erratum ibid.* **117** (2016) 079901] [arXiv:1604.06447] [INSPIRE].

[22] M. Kerner, *Next-to-leading order corrections to Higgs boson pair production in gluon fusion*, PoS(LL2016)023 [arXiv:1608.03851] [INSPIRE].

[23] S. Borowka et al., *Full top quark mass dependence in Higgs boson pair production at NLO*, *JHEP* **10** (2016) 107 [arXiv:1608.04798] [INSPIRE].

[24] G. Ferrera and J. Pires, *Transverse-momentum resummation for Higgs boson pair production at the LHC with top-quark mass effects*, *JHEP* **02** (2017) 139 [arXiv:1609.01691] [INSPIRE].

[25] M.J. Dolan, C. Englert and M. Spannowsky, *Higgs self-coupling measurements at the LHC*, *JHEP* **10** (2012) 112 [arXiv:1206.5001] [INSPIRE].

[26] J. Baglio et al., *The measurement of the Higgs self-coupling at the LHC: theoretical status*, *JHEP* **04** (2013) 151 [arXiv:1212.5581] [INSPIRE].

[27] F. Goertz, A. Papaefstathiou, L.L. Yang and J. Zurita, *Higgs boson self-coupling measurements using ratios of cross sections*, *JHEP* **06** (2013) 016 [arXiv:1301.3492] [INSPIRE].

[28] M. Gouzevitch et al., *Scale-invariant resonance tagging in multijet events and new physics in Higgs pair production*, *JHEP* **07** (2013) 148 [arXiv:1303.6636] [INSPIRE].

[29] A.J. Barr, M.J. Dolan, C. Englert and M. Spannowsky, *Di-Higgs final states augMT2ed — selecting hh events at the high luminosity LHC*, *Phys. Lett.* **B 728** (2014) 308 [arXiv:1309.6318] [INSPIRE].

[30] M.J. Dolan, C. Englert, N. Greiner and M. Spannowsky, *Further on up the road: hhjj production at the LHC*, *Phys. Rev. Lett.* **112** (2014) 101802 [arXiv:1310.1084] [INSPIRE].

[31] V. Barger, L.L. Everett, C.B. Jackson and G. Shaughnessy, *Higgs-pair production and measurement of the triscalar coupling at LHC(8,14)*, *Phys. Lett.* **B 728** (2014) 433 [arXiv:1311.2931] [INSPIRE].

[32] Q. Li, Q.-S. Yan and X. Zhao, *Higgs pair production: improved description by matrix element matching*, *Phys. Rev.* **D 89** (2014) 033015 [arXiv:1312.3830] [INSPIRE].

[33] D.E. Ferreira de Lima, A. Papaefstathiou and M. Spannowsky, *Standard model Higgs boson pair production in the $(b\bar{b})(b\bar{b})$ final state*, *JHEP* **08** (2014) 030 [arXiv:1404.7139] [INSPIRE].

[34] M. Slawinska, W. van den Wollenberg, B. van Eijk and S. Bentvelsen, *Phenomenology of the trilinear Higgs coupling at proton-proton colliders*, arXiv:1408.5010 [INSPIRE].

[35] M. Buschmann et al., *Mass effects in the Higgs-gluon coupling: boosted vs. off-shell production*, *JHEP* **02** (2015) 038 [arXiv:1410.5806] [INSPIRE].

[36] A. Azatov, R. Contino, G. Panico and M. Son, *Effective field theory analysis of double Higgs boson production via gluon fusion*, *Phys. Rev.* **D 92** (2015) 035001 [arXiv:1502.00539] [INSPIRE].

[37] D.A. Dicus, C. Kao and W.W. Repko, *Interference effects and the use of Higgs boson pair production to study the Higgs trilinear self coupling*, *Phys. Rev.* **D 92** (2015) 093003 [arXiv:1504.02334] [INSPIRE].

[38] A. Papaefstathiou, *Discovering Higgs boson pair production through rare final states at a 100 TeV collider*, *Phys. Rev.* **D 91** (2015) 113016 [arXiv:1504.04621] [INSPIRE].

JHEP08(2017)088

[39] R. Gröber, M. Mühlleitner, M. Spira and J. Streicher, *NLO QCD corrections to Higgs pair production including dimension-6 operators*, *JHEP* **09** (2015) 092 [arXiv:1504.06577] [INSPIRE].

[40] C.-T. Lu, J. Chang, K. Cheung and J.S. Lee, *An exploratory study of Higgs-boson pair production*, *JHEP* **08** (2015) 133 [arXiv:1505.00957] [INSPIRE].

[41] S. Dawson, A. Ismail and I. Low, *What's in the loop? The anatomy of double Higgs production*, *Phys. Rev.* **D 91** (2015) 115008 [arXiv:1504.05596] [INSPIRE].

[42] M. Ghezzi, R. Gomez-Ambrosio, G. Passarino and S. Uccirati, *NLO Higgs effective field theory and κ-framework*, *JHEP* **07** (2015) 175 [arXiv:1505.03706] [INSPIRE].

[43] M.J. Dolan, C. Englert, N. Greiner, K. Nordstrom and M. Spannowsky, *hhjj production at the LHC*, *Eur. Phys. J.* **C 75** (2015) 387 [arXiv:1506.08008] [INSPIRE].

[44] A. Carvalho et al., *Higgs pair production: choosing benchmarks with cluster analysis*, *JHEP* **04** (2016) 126 [arXiv:1507.02245] [INSPIRE].

[45] S. Dawson and I.M. Lewis, *NLO corrections to double Higgs boson production in the Higgs singlet model*, *Phys. Rev.* **D 92** (2015) 094023 [arXiv:1508.05397] [INSPIRE].

[46] Q.-H. Cao, B. Yan, D.-M. Zhang and H. Zhang, *Resolving the degeneracy in single Higgs production with Higgs pair production*, *Phys. Lett.* **B 752** (2016) 285 [arXiv:1508.06512] [INSPIRE].

[47] Q.-H. Cao, Y. Liu and B. Yan, *Measuring trilinear Higgs coupling in WHH and ZHH productions at the high-luminosity LHC*, *Phys. Rev.* **D 95** (2017) 073006 [arXiv:1511.03311] [INSPIRE].

[48] J.K. Behr et al., *Boosting Higgs pair production in the $b\bar{b}b\bar{b}$ final state with multivariate techniques*, *Eur. Phys. J.* **C 76** (2016) 386 [arXiv:1512.08928] [INSPIRE].

[49] H.T. Li and J. Wang, *Fully differential Higgs pair production in association with a W boson at next-to-next-to-leading order in QCD*, *Phys. Lett.* **B 765** (2017) 265 [arXiv:1607.06382] [INSPIRE].

[50] S. Kanemura, M. Kikuchi and K. Yagyu, *One-loop corrections to the Higgs self-couplings in the singlet extension*, *Nucl. Phys.* **B 917** (2017) 154 [arXiv:1608.01582] [INSPIRE].

[51] A. Agostini, G. Degrassi, R. Gröber and P. Slavich, *NLO-QCD corrections to Higgs pair production in the MSSM*, *JHEP* **04** (2016) 106 [arXiv:1601.03671] [INSPIRE].

[52] R. Gröber, M. Mühlleitner and M. Spira, *Signs of composite Higgs pair production at next-to-leading order*, *JHEP* **06** (2016) 080 [arXiv:1602.05851] [INSPIRE].

[53] S. Banerjee, B. Batell and M. Spannowsky, *Invisible decays in Higgs boson pair production*, *Phys. Rev.* **D 95** (2017) 035009 [arXiv:1608.08601] [INSPIRE].

[54] T. Huang et al., *Resonant di-Higgs production in the $b\bar{b}WW$ channel: probing the electroweak phase transition at the LHC*, arXiv:1701.04442 [INSPIRE].

[55] M. Gorbahn and U. Haisch, *Indirect probes of the trilinear Higgs coupling: $gg \to h$ and $h \to \gamma\gamma$*, *JHEP* **10** (2016) 094 [arXiv:1607.03773] [INSPIRE].

[56] G. Degrassi, P.P. Giardino, F. Maltoni and D. Pagani, *Probing the Higgs self coupling via single Higgs production at the LHC*, *JHEP* **12** (2016) 080 [arXiv:1607.04251] [INSPIRE].

JHEP08(2017)088

[57] W. Bizon, M. Gorbahn, U. Haisch and G. Zanderighi, *Constraints on the trilinear Higgs coupling from vector boson fusion and associated Higgs production at the LHC*, arXiv:1610.05771 [INSPIRE].

[58] U. Baur, T. Plehn and D.L. Rainwater, *Measuring the Higgs boson self coupling at the LHC and finite top mass matrix elements*, *Phys. Rev. Lett.* **89** (2002) 151801 [hep-ph/0206024] [INSPIRE].

[59] P. Maierhöfer and A. Papaefstathiou, *Higgs boson pair production merged to one jet*, *JHEP* **03** (2014) 126 [arXiv:1401.0007] [INSPIRE].

[60] S. Frixione, P. Nason and C. Oleari, *Matching NLO QCD computations with parton shower simulations: the POWHEG method*, *JHEP* **11** (2007) 070 [arXiv:0709.2092] [INSPIRE].

[61] S. Alioli, P. Nason, C. Oleari and E. Re, *A general framework for implementing NLO calculations in shower Monte Carlo programs: the POWHEG BOX*, *JHEP* **06** (2010) 043 [arXiv:1002.2581] [INSPIRE].

[62] J. Alwall et al., *The automated computation of tree-level and next-to-leading order differential cross sections and their matching to parton shower simulations*, *JHEP* **07** (2014) 079 [arXiv:1405.0301] [INSPIRE].

[63] V. Hirschi and O. Mattelaer, *Automated event generation for loop-induced processes*, *JHEP* **10** (2015) 146 [arXiv:1507.00020] [INSPIRE].

[64] S. Frixione and B.R. Webber, *Matching NLO QCD computations and parton shower simulations*, *JHEP* **06** (2002) 029 [hep-ph/0204244] [INSPIRE].

[65] T. Sjöstrand, S. Mrenna and P.Z. Skands, *A brief introduction to PYTHIA 8.1*, *Comput. Phys. Commun.* **178** (2008) 852 [arXiv:0710.3820] [INSPIRE].

[66] T. Sjöstrand et al., *An introduction to PYTHIA 8.2*, *Comput. Phys. Commun.* **191** (2015) 159 [arXiv:1410.3012] [INSPIRE].

[67] G. Cullen et al., GoSam*-2.0: a tool for automated one-loop calculations within the standard model and beyond*, *Eur. Phys. J.* **C 74** (2014) 3001 [arXiv:1404.7096] [INSPIRE].

[68] S.P. Jones, *Automation of 2-loop amplitude calculations*, PoS(LL2016)069 [arXiv:1608.03846] [INSPIRE].

[69] A. von Manteuffel and C. Studerus, *Reduze 2 — distributed Feynman integral reduction*, arXiv:1201.4330 [INSPIRE].

[70] S. Borowka et al., *SecDec-3.0: numerical evaluation of multi-scale integrals beyond one loop*, *Comput. Phys. Commun.* **196** (2015) 470 [arXiv:1502.06595] [INSPIRE].

[71] R. Clough and J. Tocher, *Finite element stiffness matrices for analysis of plates in bending*, in Proceedings of the *Conference on Matrix Methods in Structural Mechanics*, Wright-Patterson Air Force Base U.S.A. (1965).

[72] E. Jones, T. Oliphant and P. Peterson, *SciPy: open source scientific tools for Python*, 2001–2017.

[73] S. Catani and M.H. Seymour, *A general algorithm for calculating jet cross-sections in NLO QCD*, *Nucl. Phys.* **B 485** (1997) 291 [*Erratum ibid.* **B 510** (1998) 503] [hep-ph/9605323] [INSPIRE].

[74] R. Frederix, S. Frixione, F. Maltoni and T. Stelzer, *Automation of next-to-leading order computations in QCD: the FKS subtraction*, *JHEP* **10** (2009) 003 [arXiv:0908.4272] [INSPIRE].

JHEP08(2017)088

[75] G. Luisoni, P. Nason, C. Oleari and F. Tramontano, *$HW^{\pm}/HZ + 0$ and 1 jet at NLO with the POWHEG BOX interfaced to GoSam and their merging within MiNLO*, *JHEP* **10** (2013) 083 [arXiv:1306.2542] [INSPIRE].

[76] G. Cullen et al., *Automated one-loop calculations with GoSam*, *Eur. Phys. J.* **C 72** (2012) 1889 [arXiv:1111.2034] [INSPIRE].

[77] P. Nogueira, *Automatic Feynman graph generation*, *J. Comput. Phys.* **105** (1993) 279 [INSPIRE].

[78] J. Kuipers, T. Ueda, J.A.M. Vermaseren and J. Vollinga, *FORM version 4.0*, *Comput. Phys. Commun.* **184** (2013) 1453 [arXiv:1203.6543] [INSPIRE].

[79] G. Cullen, M. Koch-Janusz and T. Reiter, *Spinney: a Form library for helicity spinors*, *Comput. Phys. Commun.* **182** (2011) 2368 [arXiv:1008.0803] [INSPIRE].

[80] P. Mastrolia, G. Ossola, T. Reiter and F. Tramontano, *Scattering amplitudes from unitarity-based reduction algorithm at the integrand-level*, *JHEP* **08** (2010) 080 [arXiv:1006.0710] [INSPIRE].

[81] H. van Deurzen, *Associated Higgs production at NLO with GoSam*, *Acta Phys. Polon.* **B 44** (2013) 2223 [INSPIRE].

[82] T. Binoth, J.P. Guillet, G. Heinrich, E. Pilon and T. Reiter, *Golem95: a numerical program to calculate one-loop tensor integrals with up to six external legs*, *Comput. Phys. Commun.* **180** (2009) 2317 [arXiv:0810.0992] [INSPIRE].

[83] G. Cullen et al., *Golem95C: a library for one-loop integrals with complex masses*, *Comput. Phys. Commun.* **182** (2011) 2276 [arXiv:1101.5595] [INSPIRE].

[84] J.P. Guillet, G. Heinrich and J.F. von Soden-Fraunhofen, *Tools for NLO automation: extension of the golem95C integral library*, *Comput. Phys. Commun.* **185** (2014) 1828 [arXiv:1312.3887] [INSPIRE].

[85] H. van Deurzen et al., *Multi-leg one-loop massive amplitudes from integrand reduction via Laurent expansion*, *JHEP* **03** (2014) 115 [arXiv:1312.6678] [INSPIRE].

[86] T. Peraro, *Ninja: automated integrand reduction via Laurent expansion for one-loop amplitudes*, *Comput. Phys. Commun.* **185** (2014) 2771 [arXiv:1403.1229] [INSPIRE].

[87] A. van Hameren, *OneLOop: for the evaluation of one-loop scalar functions*, *Comput. Phys. Commun.* **182** (2011) 2427 [arXiv:1007.4716] [INSPIRE].

[88] V. Hirschi et al., *Automation of one-loop QCD corrections*, *JHEP* **05** (2011) 044 [arXiv:1103.0621] [INSPIRE].

[89] G. Ossola, C.G. Papadopoulos and R. Pittau, *CutTools: a program implementing the OPP reduction method to compute one-loop amplitudes*, *JHEP* **03** (2008) 042 [arXiv:0711.3596] [INSPIRE].

[90] V. Hirschi and T. Peraro, *Tensor integrand reduction via Laurent expansion*, *JHEP* **06** (2016) 060 [arXiv:1604.01363] [INSPIRE].

[91] A. Denner, S. Dittmaier and L. Hofer, *Collier: a Fortran-based complex one-loop library in extended regularizations*, *Comput. Phys. Commun.* **212** (2017) 220 [arXiv:1604.06792] [INSPIRE].

[92] F. Cascioli, P. Maierhofer and S. Pozzorini, *Scattering amplitudes with open loops*, *Phys. Rev. Lett.* **108** (2012) 111601 [arXiv:1111.5206] [INSPIRE].

JHEP08(2017)088

[93] O. Mattelaer, *On the maximal use of Monte Carlo samples: re-weighting events at NLO accuracy*, *Eur. Phys. J.* **C 76** (2016) 674 [arXiv:1607.00763] [INSPIRE].

[94] LHC Higgs Cross Section Working Group, D. de Florian et al., *Handbook of LHC Higgs cross sections: 4. Deciphering the nature of the Higgs sector*, arXiv:1610.07922 [INSPIRE].

[95] J. Butterworth et al., *PDF4LHC recommendations for LHC Run II*, *J. Phys.* **G 43** (2016) 023001 [arXiv:1510.03865] [INSPIRE].

[96] S. Dulat et al., *New parton distribution functions from a global analysis of quantum chromodynamics*, *Phys. Rev.* **D 93** (2016) 033006 [arXiv:1506.07443] [INSPIRE].

[97] L.A. Harland-Lang, A.D. Martin, P. Motylinski and R.S. Thorne, *Parton distributions in the LHC era: MMHT 2014 PDFs*, *Eur. Phys. J.* **C 75** (2015) 204 [arXiv:1412.3989] [INSPIRE].

[98] NNPDF collaboration, R.D. Ball et al., *Parton distributions for the LHC Run II*, *JHEP* **04** (2015) 040 [arXiv:1410.8849] [INSPIRE].

[99] A. Buckley et al., *LHAPDF6: parton density access in the LHC precision era*, *Eur. Phys. J.* **C 75** (2015) 132 [arXiv:1412.7420] [INSPIRE].

[100] M. Cacciari, G.P. Salam and G. Soyez, *The anti-k_t jet clustering algorithm*, *JHEP* **04** (2008) 063 [arXiv:0802.1189] [INSPIRE].

[101] M. Cacciari and G.P. Salam, *Dispelling the N^3 myth for the k_t jet-finder*, *Phys. Lett.* **B 641** (2006) 57 [hep-ph/0512210] [INSPIRE].

[102] M. Cacciari, G.P. Salam and G. Soyez, *FastJet user manual*, *Eur. Phys. J.* **C 72** (2012) 1896 [arXiv:1111.6097] [INSPIRE].

[103] S. Alioli, P. Nason, C. Oleari and E. Re, *NLO Higgs boson production via gluon fusion matched with shower in POWHEG*, *JHEP* **04** (2009) 002 [arXiv:0812.0578] [INSPIRE].

[104] S. Alioli, P. Nason, C. Oleari and E. Re, *NLO single-top production matched with shower in POWHEG: s- and t-channel contributions*, *JHEP* **09** (2009) 111 [*Erratum ibid.* **02** (2010) 011] [arXiv:0907.4076] [INSPIRE].

[105] S. Alioli, F. Caola, G. Luisoni and R. Röntsch, *ZZ production in gluon fusion at NLO matched to parton-shower*, *Phys. Rev.* **D 95** (2017) 034042 [arXiv:1609.09719] [INSPIRE].

[106] B. Hespel, F. Maltoni and E. Vryonidou, *Higgs and Z boson associated production via gluon fusion in the SM and the 2HDM*, *JHEP* **06** (2015) 065 [arXiv:1503.01656] [INSPIRE].

[107] S. Catani and B.R. Webber, *Infrared safe but infinite: soft gluon divergences inside the physical region*, *JHEP* **10** (1997) 005 [hep-ph/9710333] [INSPIRE].

[108] S. Frixione and G. Ridolfi, *Jet photoproduction at HERA*, *Nucl. Phys.* **B 507** (1997) 315 [hep-ph/9707345] [INSPIRE].

[109] M. Fontannaz, J.P. Guillet and G. Heinrich, *Is a large intrinsic k_T needed to describe photon + jet photoproduction at HERA?*, *Eur. Phys. J.* **C 22** (2001) 303 [hep-ph/0107262] [INSPIRE].

JHEP08(2017)088